Spin Crossover in [Fe(2-Picolylamine) 3] 2+ Adjusted by Organosulfonate Anions

ARTICLE *in* INORGANIC CHEMISTRY · JULY 2015

Impact Factor: 4.76 · DOI: 10.1021/acs.inorgchem.5b00870 · Source: PubMed

4 AUTHORS, INCLUDING:

Shao-Liang Zhang

Liaocheng University

16 PUBLICATIONS **64** CITATIONS

SEE PROFILE

Dong Shao

Nanjing University

9 PUBLICATIONS **37** CITATIONS

SEE PROFILE

Xinyi Wang

Nanjing University

54 PUBLICATIONS **2,680** CITATIONS

SEE PROFILE

Inorganic Chemistry

Article

pubs.acs.org/IC

Spin Crossover in $[Fe(2\text{-Picolylamine})_3]^{2+}$ Adjusted by Organosulfonate Anions

Xin-Hua Zhao, Shao-Liang Zhang, Dong Shao, and Xin-Yi Wang*

State Key Laboratory of Coordination Chemistry, Collaborative Innovation Center of Advanced Microstructures, School of Chemistry and Chemical Engineering, Nanjing University, Nanjing 210093, China

Supporting Information

ABSTRACT: Three mononuclear spin crossover (SCO) compounds $[Fe(2\text{-pic})_3]\cdot A_2\cdot Solv$ (A = *m*-ABS^-, Solv = MeOH, **1**; A = *p*-ABS^-, **2**; A = OTf^-, **3**) were prepared and characterized magnetically and structurally (2-pic = 2-picolylamine, *m*-HABS = *m*-aminobenzenesulfonic acid, *p*-HABS = *p*-aminobenzenesulfonic acid, HOTf = trifluoromethanesulfonic acid). Single-crystal X-ray analyses show that they are constructed from the charge-assisted hydrogen bonds between the 2-pic donors and the organosulfonate acceptors, forming the hydrogen-bonded three-dimensional networks for **1** and **2** and one-dimensional columns for **3**. While the $[Fe(2\text{-pic})_3]^{2+}$ cations in compounds **1** and **2** are in the meridional (mer-) configuration, it has a facial (fac-) configuration in complex **3**. Magnetic susceptibility measurements revealed the SCO transitions and the SCO properties in all three complexes are quite different. Compound **1** undergoes an abrupt SCO with critical temperatures $T_{1/2}\downarrow$ = 100 K and $T_{1/2}\uparrow$ = 103 K, while compound **2** exhibits a gradual SCO with $T_{1/2}$ = 218 K. Compound **3**, with the fac-configuration, has an abrupt SCO transition accompanied by the structural phase transition with critical temperatures $T_{1/2}\downarrow$ = 333 K and $T_{1/2}\uparrow$ = 343 K. The SCO transitions were further confirmed by the detailed structural analyses of the coordination environments of the Fe^{II} centers in both spin states and also by differential scanning calorimetry. Compared to the famous $[Fe(2\text{-pic})_3]\cdot A_2\cdot Solv$ compounds in the literature, compound **2** has the highest transition temperature for the *mer*-$[Fe(2\text{-pic})_3]^{2+}$-containing compounds, while compound **3** represents the first example of the *structurally characterized* compound of the *fac*-$[Fe(2\text{-pic})_3]^{2+}$ motif showing SCO behavior. These results show that the organosulfonate anions are very promising to adjust the hydrogen-bonded structures of the SCO compounds and improve the SCO properties of those structures.

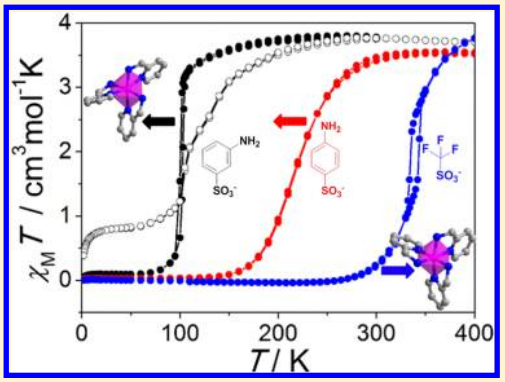

INTRODUCTION

The spin crossover (SCO) transition between a low-spin (LS) and a high-spin (HS) state is a promising way of attaining bistability at the molecular level and has attracted considerable current attention.[1,2] Accompanied by the spin state switch tuned by external stimuli, that is, temperature, pressure, light, or magnetic field, many crystal properties, such as the color, volume, dielectric constants, photoluminescence, conductivity, and so on can be finely tuned for the SCO materials, making them very attractive in thermal sensors, light switches, and information storage devices.[3]

For an SCO material, the transition temperature ($T_{1/2}$) and the detailed shape of a transition curve depend on the ligand-field strength and the cooperative effect. In the solid state, cooperativity is probably the most difficult to design and control as it is usually governed by the intermolecular interactions such as hydrogen bond (H-bond), $\pi-\pi$ interaction, and van der Waals interaction. More recently, the stronger coordination bonds were also used to construct SCO materials of strong cooperative effects.[4] Among all these interactions, the H-bonds have been shown to have a remarkable influence on the SCO properties by adjusting the ligand field strength and the cooperative effect.[5−8] As an illustrative example, the efficient H-bonds between the ligand and the imidazole group in compound $[FeL(HIm)_2]$ (L is a ligand with a N_2O_2 pocket) led to the formation of the two-dimensional (2D) hydrogen-bonded network and very strong cooperativity with a 70 K wide hysteresis loop.[5a,b] Also, it was found that in the various mononuclear $[FeL_n(NCS)_2]$ complexes with an FeN_6 environment, there is a direct correlation between the abruptness of the transition and the S···H−C contacts.[5d] In addition, for the heteroleptic iron(II) complexes $[(H_2bip)_2Fe(pic)]X_2$ (X = anions, H_2bip = 2,2′-bi-1,4,5,6-tetrahydropyrimidine), the magnetic behavior was found to be heavily influenced by different H-bonds between the ligands and different anions.[6] Furthermore, the influence of the H-bond on the SCO properties is not limited to mononuclear complexes. For example, in the one-dimensional (1D) Fe(II)-1,2,4-triazole coordination polymers, wide thermal hysteresis loops around room temperature are also associated with the hydrogen-bonded networks.[7a,b] In addition, the guest−host H-bonds

Received: April 21, 2015

DOI: 10.1021/acs.inorgchem.5b00870
Inorg. Chem. XXXX, XXX, XXX−XXX

involving the guest and the framework were found to play an important role on the SCO properties of many metal organic frameworks, such as the 2D networks of $[Fe(btr)_2(NCS)_2]\cdot H_2O$[8a] and $[Fe(bped)_2(NCS)_2]\cdot 3EtOH$[8b] and the three-dimensional (3D) Hoffman-like coordination polymers $[Fe(2,5\text{-bpp})\{Au(CN)_2\}_2]\cdot x$Solv.[8c]

Despite the paramount importance of the H-bonds to the valuable SCO properties, the design and even the control of the H-bonds in the SCO compounds are still challenging. In most SCO systems, the H-bonds are introduced in a more or less serendipitous way. Generally, they are randomly formed between the suitable components, such as the ligands to the solvents and anions and so on. Given the pivotal role the H-bonds play in the SCO materials, the rational design and control of the H-bonds deserve further efforts. Meanwhile, because of its strength and directionality, H-bond has been exploited extensively in the supramolecular chemistry, such as the geometric and conformational control on the molecule level and the construction of flexible frameworks.[9,10] For example, from the charge-assisted H-bonds between the guanidinium cation $[C(NH_2)_3]^+$ and the organosulfonate anions, a huge amount of inclusion compounds (more than 450 reported) containing different guest molecules have been reported.[11,12] Interestingly, the guanidinium cation can be replaced by cationic metal complexes where the ligands (such as ammonia, water, and various ammines) can provide protons for hydrogen bonding.[13] Along this line of second sphere interaction, one of us has reported a series of flexible hydrogen-bonded metal complex−sulfonate frameworks holding various guest molecules in the cavity.[14]

By replacing the diamagnetic metal ions with the SCO active centers, these hydrogen-bonded frameworks can provide a good platform for the SCO materials. For this purpose, the $[Fe(2\text{-pic})_3]^{2+}$ (2-pic = 2-picolylamine) cation represents an ideal system, not only because of the rich protons from three NH_2 groups for hydrogen bonding but also because of their intriguing SCO properties. Actually, the study of the SCO properties of the $[Fe(2\text{-pic})_3]\cdot A_2\cdot$Solv (A = anions, Solv = Solvent) compounds can be traced to the 1960s, and these compounds have played a prominent role in the development of SCO research, especially on the understanding of the role of H-bonds on the SCO properties.[15−19] Structurally, there are two different geometries of the $[Fe(2\text{-pic})_3]^{2+}$ center: *mer*-$[Fe(2\text{-pic})_3]^{2+}$ in most of the reported examples[15a,b,16c,d,17] and *fac*-$[Fe(2\text{-pic})_3]^{2+}$ in $[Fe(2\text{-pic})_3]\cdot Cl_2\cdot 2H_2O$[16a,b] and $[Fe(2\text{-pic})_3]\cdot I_2$[15c] (Scheme 1). Magnetically, their SCO properties can be elegantly tuned by different counterions (Cl^-, Br^-, I^-)[15] and solvent molecules incorporated in the structure (water, methanol, ethanol, 1-propanol, 2-propanol, *tert*-butanol, and allyl-alcohol).[16,17] Generally, the $T_{1/2}$ values of the *mer*-$[Fe(2\text{-pic})_3]^{2+}$ compounds are usually below 150 K, while the SCO properties of the *fac*-$[Fe(2\text{-pic})_3]^{2+}$ compounds depend strongly on the number of the lattice water molecules. While the $[Fe(2\text{-pic})_3]\cdot Cl_2\cdot 2H_2O$ remains LS at room temperature, the $[Fe(2\text{-pic})_3]\cdot Cl_2\cdot H_2O$ has a thermally induced SCO with a 91 K wide hysteresis loop ($T_{1/2}\downarrow$ = 204 K and $T_{1/2}\uparrow$ = 295 K), which was observed first by ^{57}Fe Mössbauer spectroscopy[16a] and was later found to be caused by the existence of a metastable LS phase.[18]

Given the aforementioned consideration, we chose the organosulfonate derivatives as the counteranions in the $[Fe(2\text{-pic})_3]^{2+}$ system, hoping to gain more control over their hydrogen-bonded SCO frameworks and SCO properties via the different sizes and shapes of the large amount of organosulfonates. Herein we report the syntheses, structures at both LS and HS states, thermal analyses, and SCO properties of three $[Fe(2\text{-pic})_3]\cdot A_2\cdot$Solv compounds with three monosulfonates.

Scheme 1. Structures of *mer*-$[Fe(2\text{-pic})_3]^{2+}$ and *fac*-$[Fe(2\text{-pic})_3]^{2+}$ Metal Complexes and the Organosulfonate Anions Used to Prepare Compounds 1−3

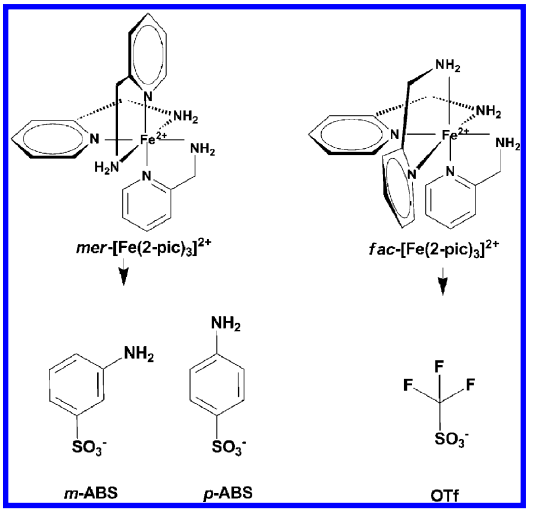

EXPERIMENTAL SECTION

Physical Measurements. Infrared spectral samples were prepared as KBr pellets, and the spectra were obtained over the range of 4000−400 cm^{-1} on a Bruker Tensor 27 FT-IR spectrometer. Elemental analyses were performed on an Elementar Vario EL III elemental analyzer. Thermal analyses above room temperature for compound **1** were performed on a Netzsch STA 449 C Simultaneous Thermal Analyzer at a rate of 10 K min^{-1} under a N_2 atmosphere. Differential scanning calorimetry measurements were recorded using a METTLER-TOLEDO DSC1 differential scanning calorimeter with temperature sweep rates of 10 K min^{-1} for compound **2** and 1, 2, 5, and 10 K min^{-1} for compound **3**. Power X-ray diffraction (PXRD) patterns of **1**−**3** were recorded on a Bruker D8 Advance diffractometer with a Cu Kα X-ray source (operated at 40 kV and 40 mA) at several different temperatures. Magnetic measurements were performed on a Quantum Design SQUID VSM magnetometer under a field of 0.1 T in the temperature range from 2 to 400 K. Experimental susceptibilities were corrected for diamagnetism of the sample holders and that of the compounds according to Pascal's constants.

Materials and Syntheses of Compounds 1 to 3. The starting materials, including $FeSO_4\cdot 7H_2O$, Fe powder, 2-pic, *m*-aminobenzenesulfonic acid (*m*-HABS), *p*-aminobenzenesulfonic acid (*p*-HABS), and trifluoromethanesulfonic acid (HOTf) were used as purchased without further purification. Deoxygenated solvents were prepared by bubbling them with nitrogen for 1 h or distilling under nitrogen. All the synthesis procedures and all product handling were performed in a nitrogen atmosphere to avoid the possible oxidation of Fe^{II} ion. $Fe(OTf)_2\cdot 2CH_3CN$ was prepared according to a published method.[20]

$[Fe(H_2O)_6]\cdot(m\text{-}ABS)_2$. A 10 mL aliquot of aqueous solution containing 1.39 g of $FeSO_4\cdot 7H_2O$ (5 mmol) was mixed with 10 mL of aqueous solution of NaOH (0.4 g, 10 mmol). The resulting mixture was stirred at room temperature for 10 min and then filtrated. The residue was added to 15 mL of H_2O containing 0.86 g of *m*-ABS (5 mmol), and the resulting mixture was stirred for 10 min and then filtrated to remove the remaining insoluble material. The pale yellow filtrate was concentrated under vacuum at 80 °C to 3 mL and cooled to room temperature to obtain white crystals. The crystals were collected by filtration and washed with cold water to give 0.44 g (35%)

DOI: 10.1021/acs.inorgchem.5b00870
Inorg. Chem. XXXX, XXX, XXX−XXX

Table 1. Crystallographic Data and Structure Refinement Parameters for Compounds 1−3

	1		2			3		
formula	$C_{31}H_{40}FeN_8O_7S_2$		$C_{30}H_{36}FeN_8O_6S_2$			$C_{20}H_{24}F_6FeN_6O_6S_2$		
fw, g mol^{-1}	756.68		724.64			678.42		
T, K	90	120	120	370	120	320	360	400
crystal system	monoclinic	monoclinic	monoclinic	monoclinic	triclinic	triclinic	triclinic	triclinic
space group	$P2_1/c$	$P2_1/c$	$P2_1/c$	$P2_1/c$	$P\bar{1}$	$P\bar{1}$	$P\bar{1}$	$P\bar{1}$
a, Å	17.750(4)	18.032(4)	12.5927(2)	13.0398(2)	7.3928(8)	7.5337(1)	7.625(1)	7.687(1)
b, Å	11.468(2)	11.313(2)	13.5534(2)	13.5849(2)	10.6332(2)	10.7234(1)	11.616(2)	11.519(2)
c, Å	16.650(3)	16.684(3)	18.363(3)	18.575(3)	17.5912(2)	17.7641(1)	17.52(2)	17.66(2)
α, deg	90.00	90.00	90.00	90.00	75.8260(1)	75.3990(1)	70.742(2)	70.343(2)
β, deg	96.684(3)	95.747(3)	90.481(2)	90.588(2)	88.6760(1)	89.5900(1)	80.735(2)	80.392(2)
γ, deg	90.00	90.00	90.00	90.00	82.1590(1)	81.8790(1)	81.149(2)	80.945(2)
V, Å^3	3366.2(1)	3386.3(1)	3133.9(8)	3290.2(8)	1328.1(3)	1374.2(3)	1437(3)	1443(3)
Z	4	4	4	4	2	2	2	2
F(000)	1584	1584	1512	1512	692	692	692	692
crystal size	0.20 × 0.15 × 0.13		0.40 × 0.38 × 0.25			0.54 × 0.45 × 0.32		
T_{min}, T_{max}	0.5806, 0.7456	0.6681, 0.7456	0.3887, 0.7456	0.4319, 0.7456	0.4918, 0.7456	0.4874, 0.7456	0.4333, 0.7456	0.3840, 0.7456
R_1, wR_2 $[I \geq 2\sigma(I)]$[a]	0.0536, 0.1316	0.0491, 0.1121	0.0334, 0.1035	0.0423, 0.1015	0.0356, 0.0987	0.0450, 0.1199	0.0779, 0.1961	0.0937, 0.2480
GOF	1.022	1.021	1.041	1.023	1.138	1.054	1.034	1.014
$\Delta\rho$,[b] e/ Å^3	0.725, −0.862	0.537, −0.621	0.409, −0.692	0.403, −0.283	0.949, −0.978	0.584, −0.602	0.776, −0.553	1.036, −0.438

[a] $R_1 = \sum||F_o| - |F_c||/\sum|F_o|$; $wR_2 = \{\sum_w[(F_o^2 - F_c^2)^2]/\sum[_w(F_o^2)^2]\}^{1/2}$. [b] Maximum and minimum residual electron density.

of product. Elem anal. (%) calcd (found) for $C_{12}H_{24}N_2S_2FeO_{12}$: C, 28.36 (28.31); H, 4.76 (4.95); N, 5.51 (5.44). IR (KBr, cm^{-1}): 3380(b, s), 1653(m), 1625(s), 1595(s), 1488(s), 1454(m), 1317(s), 1282(m), 1195(s), 1038(s), 988(m), 861(m), 788(s), 710(s), 684(s), 612(s), 532(m).

[Fe(H$_2$O)$_6$]·(p-ABS)$_2$. This compound was synthesized by a similar method as that for $[Fe(H_2O)_6]\cdot(m\text{-ABS})_2$ by using *p*-ABS (0.86 g, 5 mmol). Yield: 0.50 g, 39%. Elem anal. (%) calcd (found) for $C_{12}H_{24}N_2S_2FeO_{12}$: C, 28.36 (27.64); H, 4.76 (4.47); N, 5.51 (5.36). IR (KBr, cm^{-1}): 3396(b, s), 1655(m), 1631(s), 1600(m), 1503(s), 1434(m), 1317(m), 1177(s), 1124(s), 1034(s), 1000(s), 822(s), 695(s), 569(s).

*[Fe(2-pic)$_3$]·(m-ABS)$_2$·MeOH (**1**).* A 2 mL methanol solution containing 0.1 mmol of $[Fe(H_2O)_6]\cdot(m\text{-ABS})_2$ (51 mg) was mixed with 2 mL of methanol solution of 2-pic (50 mg, 0.45 mmol). The resulting solution was then filtrated and added to a test tube. Diethyl ether vapor was then allowed to diffuse into the test tube. Brown-yellow block single crystals formed in the tube in 2 d. The crystals were then removed from the test tube and washed with small amount of methanol. Yield: 50 mg, 66% based on the starting ferrous salt. Elem anal. (%) Calcd (found) for $C_{31}H_{40}FeN_8O_7S_2$: C, 49.21 (49.03); H, 5.33 (5.36); N, 14.81 (14.86). IR (KBr, cm^{-1}): 3419(m), 3344(m), 3292(b, s), 1600(s), 1486(s), 1440(s), 1184(s), 1034(s), 775(s), 706(s), 619(s). The desolvated sample of **1** was obtained by heating **1** in vacuum at 90 °C for 1 h. Elem anal. (%) Calcd (found) for $C_{30}H_{36}FeN_8O_6S_2$: C, 49.72 (49.55); H, 5.01 (5.26); N, 15.46 (15.82). IR (KBr, cm^{-1}): 3414(s), 3213(b, s), 1607(s), 1483(m), 1442(m), 1440(s), 1187(s), 1035(s), 990(s), 767(s), 709(s), 619(s).

*[Fe(2-pic)$_3$]·(p-ABS)$_2$ (**2**).* **2** was prepared by a similar procedure as that for **1** by using $[Fe(H_2O)_6]\cdot(p\text{-ABS})_2$ (51 mg, 0.1 mmol). Brown-yellow block single crystals formed in the tube in 2 d. Yield: 30 mg, 41%. Elem anal. (%) Calcd (found) for $C_{30}H_{36}FeN_8O_6S_2$: C, 49.72 (49.55); H, 5.01 (5.09); N, 15.46 (15.42). IR (KBr, cm^{-1}): 3413(m), 3270(m), 1601(s), 1501(m), 1438(m), 1293(m), 1195(s), 1121(s), 1028(s), 827(m), 770(m), 695(s), 575(s).

*[Fe(2-pic)$_3$]·(OTf)$_2$ (**3**).* Compound **3** was prepared by a similar method as that for **1** by using $Fe(OTf)_2\cdot 2CH_3CN$ (44 mg, 0.1 mmol) in the acetonitrile solution. Dark red block crystals formed in the tube over the period of two weeks. Yield: 40 mg, 72%. Elem anal. (%) Calcd (found) for $C_{20}H_{24}F_6FeN_6O_6S_2$: C, 35.41 (35.51); H, 3.57 (3.81); N, 12.39 (12.41). IR (KBr, cm^{-1}): 3307(m), 3278(m), 1609(m), 1480(m), 1448(m), 1277(s), 1256(s), 1156(s), 1030(s), 772(s), 638(s), 574(m), 517(m).

X-ray Crystallography. Single-crystal X-ray Diffraction measurements of **1**−**3** were performed on an APEX DUO diffractometer with a CCD area detector (Mo Kα radiation, λ = 0.710 73 Å) under a nitrogen flow. For all of them, X-ray data at different temperatures (90 and 120 K for **1**, 120 and 370 K for **2**, and 120, 320, 360, and 400 K for **3**) were collected using a same single crystal. For all the data sets of compounds **1** and **2** and the 120 and 320 K data sets of compound **3**, the APEX^{II} program was used to determine the unit cell parameters and for data collection. For the 360 and 400 K data sets of compound **3**, the program Cell_NOW[21] was used to determine the unit cells with all the unit cell angles lower than 90°. Data were integrated using SAINT and SADABS.[22] The structures of all the compounds were solved by direct methods and refined by full matrix least-squares methods based on F^2 using the SHELXTL program.[23] All non-hydrogen atoms were refined anisotropically, and all hydrogen atoms were refined by the riding mode. Details of the data collections and structural refinement parameters are provided in Table 1. Selected bond lengths and bond angles for **1**−**3** are listed in Supporting Information, Tables S1−S3. The details of the hydrogen bonds are listed in Supporting Information, Tables S4−S6. Additional crystallographic information is available in the Supporting Information.

Furthermore, the purity of compounds **1** to **3** as well as the desolvated sample of **1** and the structural phase transition of **3** were further investigated by PXRD (Supporting Information, Figures S1−3). The experimental PXRD patterns of **1** and **2** are in good agreement with their simulated spectra, indicating the phase purities and stabilities. For **3**, the PXRD patterns were measured at two temperatures, namely, 320 and 360 K. As shown in Supporting Information, Figure S3, the spectra at the HS phase shows significant changes compared to the LS phase. For example, the diffraction peak at $2\theta \approx 8.7°$ shifts to $2\theta \approx 8.3°$, and the peak at $2\theta \approx 10.3°$ disappears. These results suggest that **3** undergoes a structural phase transition, which is consistent with the single-crystal structural analyses of **3**.

RESULTS

Crystal Structures. The structures of all three compounds were solved by single-crystal X-ray diffraction. All of them are supramolecular networks sustained by extensive hydrogen-bond interactions between the amine donors of the Fe^{II} complexes (and also of the *m*-ABS$^-$ and *p*-ABS$^-$ anions) and the diamagnetic organosulfonate acceptors. To investigate the structural changes accompanied by the SCO transition, their

DOI: 10.1021/acs.inorgchem.5b00870
Inorg. Chem. XXXX, XXX, XXX−XXX

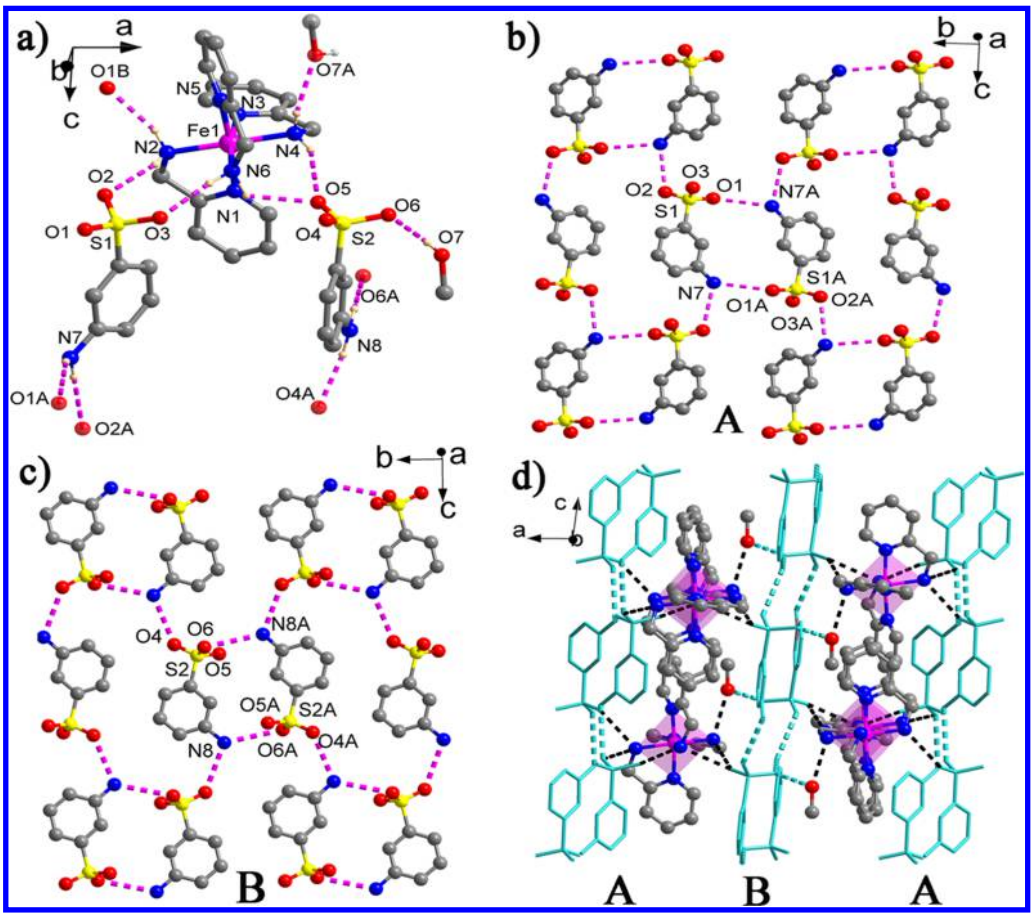

Figure 1. Hydrogen-bonding environments of the *mer*-$[Fe(2\text{-pic})_3]^{2+}$ metal complex (a), the hydrogen-bonded anionic 2D layers of *m*-ABS^- along the *bc* plane (b, c), and the crystal packing (d) of compound **1** at 90 K. Dashed lines represent hydrogen bonds.

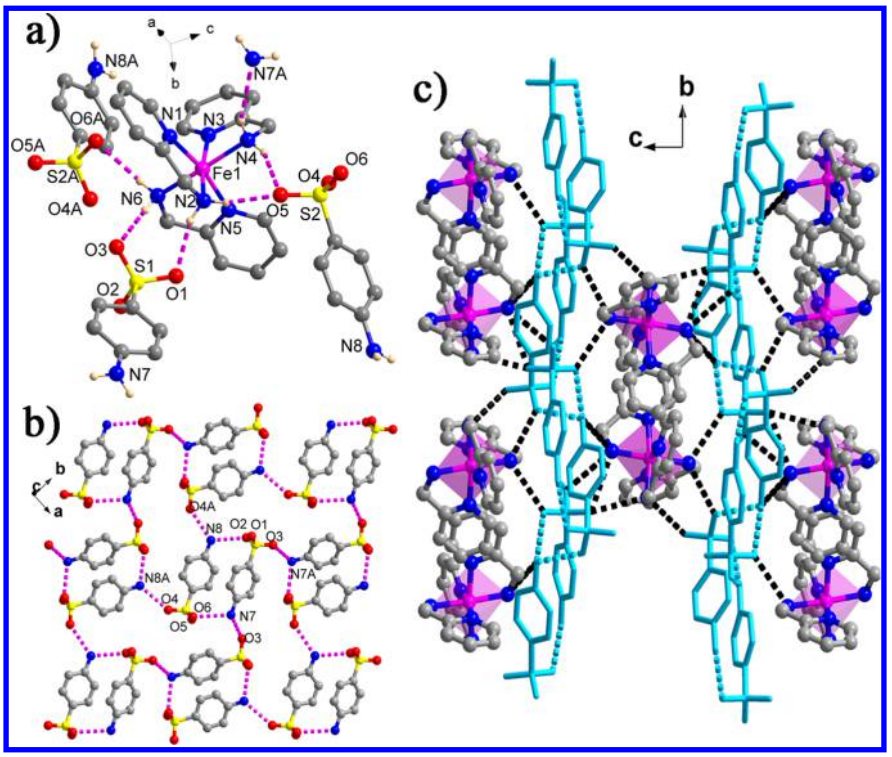

Figure 2. Hydrogen-bonding environments of the *mer*-$[Fe(2\text{-pic})_3]^{2+}$ metal complex (a), the hydrogen-bonded anionic 2D layer of *m*-ABS^- along the *ab* plane (b), and the crystal packing (c) of compound **2** at 120 K. Dashed lines represent hydrogen bonds.

DOI: 10.1021/acs.inorgchem.5b00870
Inorg. Chem. XXXX, XXX, XXX−XXX

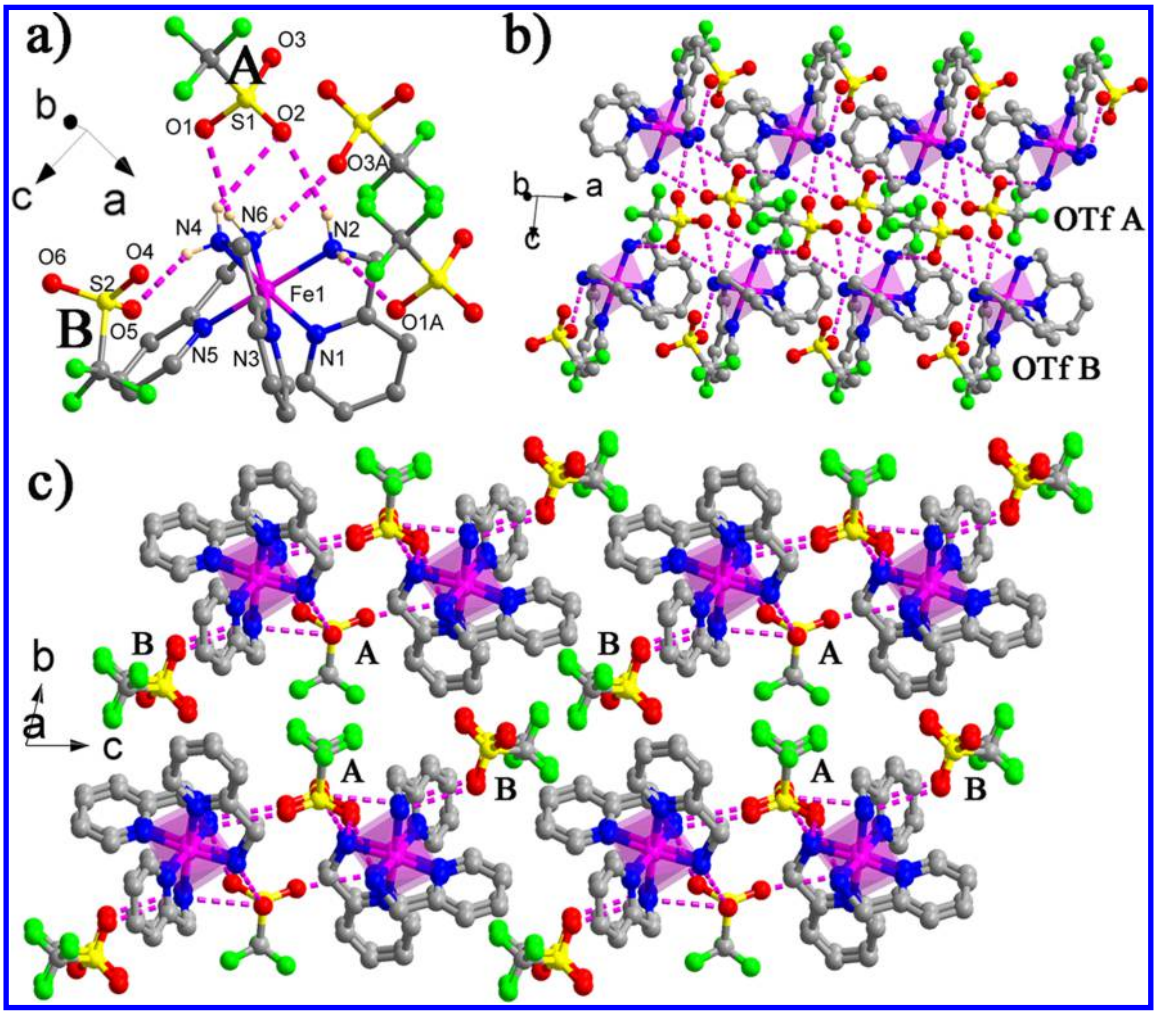

Figure 3. Hydrogen-bonding environments of the *fac*-$[Fe(2\text{-pic})_3]^{2+}$ metal complex (a), the hydrogen-bonded 1D columns running along the *a* axis (b), and the crystal packing (c) of compound **3** at 120 and 320 K. Dashed lines represent hydrogen bonds.

structures were all collected at different temperatures (90 and 120 K for **1**, 120 and 370 K for **2**, and 120, 320, 360, and 400 K for **3**). In the following discussion, their low-temperature structures will be analyzed and described first, and the comparison of the structures at different temperatures will be discussed later.

Compound **1** crystallized into a monoclinic space group $P2_1/c$, and its unique unit consists of one *mer*-$[Fe(2\text{-pic})_3]^{2+}$ cation, two *m*-ABS^- counteranions, and one crystallized methanol molecule, as depicted in Figure 1. The Fe^{II} ion has an octahedral coordination environment with six nitrogen atoms from three 2-pic ligands in the mer-configuration. The Fe—N(pyridine) distances are slightly shorter than the Fe—N(amine) distances, consistent with the reported examples and reflecting the significant interactions between the t_{2g} orbitals on the LS Fe^{II} with pyridine π orbitals. As anticipated, abundant H-bonds were found in the structure (Figure 1a and Supporting Information, Table S4). First of all, because the *m*-ABS^- anion contains both the H-bond donor (NH_2) and H-bond acceptor (SO_3), H-bonds were found among *m*-ABS^- anions (N7···O1A = 2.980 Å, N7···O2A = 3.056 Å, N8···O4A = 2.970 Å, N8···O6A = 3.143 Å), efficiently forming 2D anionic networks along the *bc* plane (Figure 1b,c). Interestingly, every 2D layer is formed by only one crystallographic unique *m*-ABS^- anion (layer A and layer B). In addition, all three NH_2 groups in the *mer*-$[Fe(2\text{-pic})_3]^{2+}$ cation act as H-donors to two different sulfonate anions, forming another set of hydrogen bonds (N2···O2 = 2.979 Å, N6···O3 = 3.019 Å, N4···O5 = 3.015 Å, N6···O5 = 2.923 Å, Figure 1a). These hydrogen bonds connect the *mer*-$[Fe(2\text{-pic})_3]^{2+}$ cations to the anionic 2D layers of *m*-ABS^- along the *a* direction and form the 3D framework of **1** (Figure 1d). The solvated methanol molecules also participated in the formation of H-bonds between the sulfonates and the 2-pic ligands (O7···O6 = 2.766 Å, N4···O7 = 2.966 Å), serving as additional linkers between the anions and the cations. Actually, because of these H-bond interactions, the methanol molecule is quite stable in the structure up to 390 K. As can be seen from the thermogravimetric analysis (TGA, Supporting Information, Figure S4), the decrease in mass (4.0%) in the temperature range of 390−440 K corresponds to the removal of the crystallized methanol molecules (calc. 4.2%). Also, the PXRD spectrum for the desolvated **1** (Supporting Information, Figure S1) does not change much compared to that of **1**, suggesting that the structure of **1** does not change significantly during the desolvation.

Because of the very similar organosulfonate anion, the crystal structure of **2** is quite similar to that of **1**. It also crystallized into a monoclinic space group $P2_1/c$. In the asymmetric unit of **2**, there are one *mer*-$[Fe(2\text{-pic})_3]^{2+}$ cation and two *p*-ABS^- counteranions. No lattice solvent molecule was found in the

DOI: 10.1021/acs.inorgchem.5b00870
Inorg. Chem. XXXX, XXX, XXX−XXX

structure. The Fe^{II} ion is also in an octahedral coordination environment of the *mer*-configuration of the 2-pic ligands. As we can see in Figure 2, various hydrogen bonds were also responsible for the formation of the 3D network. The details of the hydrogen bonds were listed in Supporting Information, Table S5. Similar to **1**, two crystallographically unique *p*-ABS^- anions are connected to each other by the H-bonds between the NH_2 and SO_3 groups of the anions, forming anionic 2D networks along the *ab* plane (Figure 2b). Different from **1**, the 2D layer of **2** contains both *p*-ABS^- anions, and there is only one type of 2D layer in **2**. As for the *mer*-$[Fe(2\text{-pic})_3]^{2+}$ cation, all of the six hydrogen atoms from the NH_2 groups of three 2-pic ligands were found to participate in the formation of the H-bonds, not only to the SO_3 groups of *p*-ABS^- but also to the NH_2 group of the *p*-ABS^- anion. Thus, the *mer*-$[Fe(2\text{-pic})_3]^{2+}$ cations interact with the 2D anionic layers very efficiently, leading to self-assembling of the stable hydrogen-bonded framework by alternating layers of the cations and anions along the *c* axis (Figure 2c).

As for compound **3**, it crystallized into the triclinic space group $P\bar{1}$, and its asymmetric unit consists of one *fac*-$[Fe(2\text{-pic})_3]^{2+}$ cation and two OTf^- counteranions. As in **2**, no lattice solvent molecule was found in **3**. Different from **1** and **2**, the three NH_2 groups of the 2-pic ligands form a triangular face of the octahedron, which leads to the *fac*-configuration of the coordination environment of the Fe^{II} center (Figure 3a). All six hydrogen atoms of the three NH_2 groups are H-bond donors to the neighbor SO_3 groups of four OTf^- anions (Figure 3a, Supporting Information, Table S6). Since there is no H-bond donor group in the OTf^- anion, H-bonds are only found between the OTf^- and NH_2 groups. One OTf^- anion (denoted as anion A, Figure 3a) uses all three oxygen atoms (O1, O2, and O3), and the other (denoted as anion B) uses only one oxygen atom (O5) to form the H-bonds. Linked by the H-bonds involving only the anion A, the structure of **3** can be described as 1D columns running along the *a* axis (Figure 3b). Inside this column, the connection between the *fac*-$[Fe(2\text{-pic})_3]^{2+}$ cation and the SO_3 group of anion A closely resembles the interaction between the famous ganidinium–sulfonate system: both the SO_3 and metal complexes connect to three adjacent units using the charge-assisted H-bonds. These 1D columns are then packed together by the van der Waals interaction, separating to each other by the hydrogen-bonded sulfonate anions B (Figure 3c).

As we stated above, the structures of **1**–**3** were solved at different temperatures below and above their SCO transition temperatures. As for **1**, although the space group remains the same, the high-temperature phase contains one disordered *m*-ABS^- anion where the SO_3 group is disordered in two positions. For compound **2**, both the space group and the structure are very similar for the HT and LT phases. As for **3**, although the space group does not change during the SCO transition, the unit cell parameters change significantly for the HT and LT phases, indicating a crystallographic phase transition for compound **3**. As can be seen in Table 1, the α and β values are almost 5° and 9° smaller in the HT phase. At the same time, the power XRD spectra for **3** at 320 and 360 K also confirmed the structural phase transition (Supporting Information, Figure S3). As expected, the OTf^- anions show considerable disorder in the HT phase. Interestingly, the extent of disorder is of remarkable difference for the two OTf^- anions because of the difference of the hydrogen-bond interactions involved. For OTf^- anion A, although the CF_3 group is disordered in two positions, the SO_3 group is not disordered at all because it is "fixed" by a series of N–H···O H bonds (Figure 4 and Supporting Information, Table S6). Meanwhile, for anion

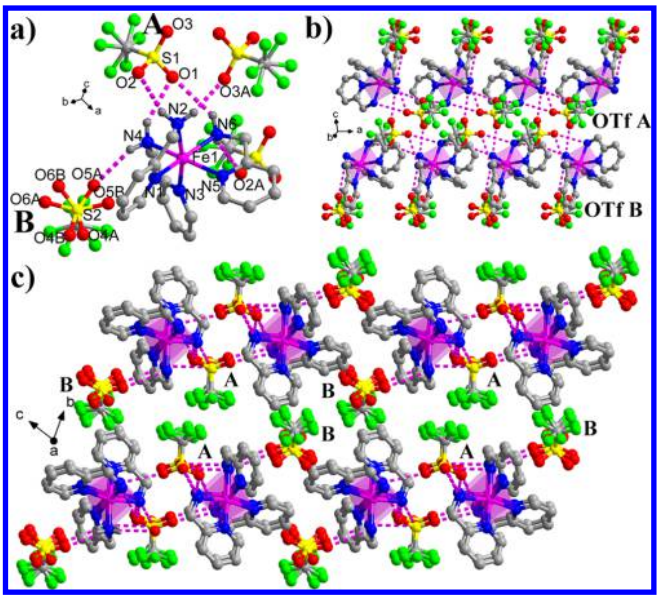

Figure 4. Hydrogen-bonding environments of the *fac*-$[Fe(2\text{-pic})_3]^{2+}$ metal complex (a), the hydrogen-bonded 1D columns running along the *a* axis (b), and the crystal packing (c) of compound **3** at 360 and 400 K. Dashed lines represent hydrogen bonds.

B, both the CF_3 and SO_3 groups are disordered in two positions as there is only one weak N–H···O hydrogen bond for its SO_3 group. Besides, although the resulting 1D H-bonded columns are similar in both the LT and HT phases, the OTf^- anion B rotates significantly in the HT phase compared to that in the LT phase (Figure 4). As the main difference between the LT and HT phases lies in the order or disorder of the triflate anions, we think that this order–disorder transition should be the origin of the structural phase transition and of paramount importance to the observed hysteresis loops of **3** (vide post).

Most importantly for our investigation, several structural parameters of the Fe^{II} centers for both the LT and HT phases of **1**–**3** are listed in Table 2. These parameters include the average Fe–N bond length, the distortion parameters $\sum$ and Θ ($\sum$ is defined as the sum of the deviation from 90° of the 12 N–Fe–N angles of the FeN_6 octahedron, and Θ is the sum of the deviation from 60° of the 24 trigonal angles of the projection of the FeN_6 octahedron onto its trigonal faces),[24] the continuous shape measures (CShM's) of the Fe^{II} centers relative to the ideal octahedron calculated by SHAPE 2.1,[25] and the octahedral volumes of the Fe^{II} centers. As the SCO transition from HS to LS Fe^{II} centers leads to the depopulation of the antibonding e_g* orbitals, the Fe–N bonds are strengthened, and the LS Fe^{II} centers generally adopt more regular coordination geometry than their HS counterparts. This leads to the shorter Fe–N bonds, lower $\sum$ and Θ values, smaller octahedral volumes, and lower CShM's for the LS state. As we can see in Table 2, the increase of the average Fe–N bond lengths is ~0.2 Å for all three compounds, typical for an Fe^{II} compound with SCO transition. Also, all these parameters have smaller values in the LT phase and increase significantly when the temperature increases, which is very typical for the SCO transition. Furthermore, we can see that at 120 K, the $\sum$ and Θ values for compound **3** are smaller than those values of **2**

DOI: 10.1021/acs.inorgchem.5b00870
Inorg. Chem. XXXX, XXX, XXX–XXX

Table 2. Structure Parameters of 1−3 at Various Temperatures

compound	1		2		3			
	90 K	120 K	120 K	370 K	120 K	320 K	360 K	400 K
Fe−N [Å]	2.016	2.185	2.003	2.192	1.998	2.026	2.155	2.170
∑ [deg]	54.46	91.57	52.71	87.11	51.19	56.90	81.68	86.20
Θ [deg]	85.69	155.59	85.49	143.59	74.96	84.50	125.10	131.48
CShM's	0.679	2.184	0.676	1.796	0.520	0.651	1.429	1.605
octahedral volume [Å^3]	10.756	13.312	10.582	13.586	10.516	10.925	12.961	13.208

at the same temperature, which suggests that the *fac*-[Fe(2-pic)$_3$]$^{2+}$ center in **3** displays a relatively less distorted geometry and tend to stay in the LS state as compared to **2**. As we can see below, the modifications of these structural parameters are all consistent with the magnetic measurements.

Magnetic Properties. The magnetic susceptibilities of the finely ground powders of the single-crystal samples of all three compounds were measured under the ambient pressure using the settle mode. The samples of compounds **1** to **3** were cooled from room temperature to 2 K, and then the magnetic susceptibilities were measured in the warming mode and then in the cooling mode to 2 K, while the magnetic susceptibility of the desolvated samples of compound **1** was recorded in the cooling mode from 400 to 2 K and then in the warming mode to 400 K (Figure 5). To study the scan rate effects on the thermal hysteresis loop of **3**, the susceptibility data of **3** were also measured using the sweep mode with different temperature sweep rates of 1, 2, 5, and 10 K min^{-1} (Figure 6). The details of the measurements and the obtained parameters for the susceptibility measurements were listed in Supporting Information, Table S7.

For compound **1**, the $\chi_M T$ value at low temperature is close to zero (0.16 cm^3 mol^{-1} K at 80 K), confirming the LS state. At ∼100 K, the $\chi_M T$ value increases abruptly, reaching a value of 3.37 cm^3 mol^{-1} K at 120 K, and increases very slowly to a value of 3.76 cm^3 mol^{-1} K at 300 K, consistent with the value for a magnetic anisotropic HS Fe^{II} ion (Figure 5a). Therefore, **1** undergoes an abrupt and complete SCO transition. Two subsequent cooling−heating cycles suggest the presence of a stable thermal hysteresis loop with 3 K width ($T_{1/2}\downarrow$ = 100 K and $T_{1/2}\uparrow$ = 103 K). In addition, as the methanol molecules in **1** begin to escape at 390 K as suggested by the TGA data (Supporting Information, Figure S4), the magnetic susceptibility of the desolvated sample of **1** was also recorded. As we can see, as the temperature decreases from 400 K, and the $\chi_M T$ value remains almost constant to 250 K and then decreases more gradually from 3.52 cm^3 mol^{-1} K to 0.76 cm^3 mol^{-1} K at 60 K. When cooled further, the $\chi_M T$ values remain almost constant until 20 K and decrease further to 2 K. The transition temperature is $T_{1/2}\downarrow \approx$ 110 K. The $\chi_M T$ value at 60 K indicates that ∼20% of the Fe^{II} centers still remain in the HS state, and the final decrease below 20 K is attributed to the zero-field splitting of residual HS Fe^{II} centers. The presence of the intermolecular antiferromagnetic coupling between the Fe^{II} centers is very unlikely as the spin centers are well isolated with the shortest Fe−Fe distance of 9.425 Å. The $\chi_M T$ data were measured again in the warming mode to 400 K and suggest that there is no hysteresis loop for the desolvated sample of **1**. This incomplete and more gradual SCO behavior of the desolvated sample highlights the importance of the hydrogen-bonded methanol to the SCO property of **1**.

In the case of **2**, the $\chi_M T$ value is only 0.02 cm^3 mol^{-1} K at 2 K, consistent with a LS Fe^{II} center. When the sampe is heated,

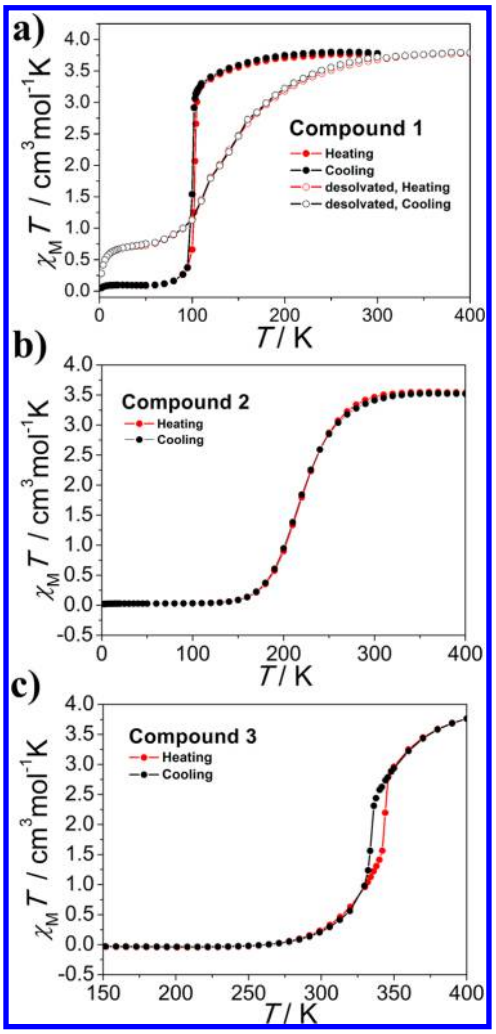

Figure 5. Temperature-dependent $\chi_M T$ plots for **1** (a), **2** (b), and **3** (c) measured in the settle mode.

the $\chi_M T$ value remains nearly constant until 150 K, gradually increases to 3.41 cm^3 mol^{-1} K at 300 K, and finally reaches 3.52 cm^3 mol^{-1} K at 400 K (Figure 5b). Thus, compound **2** undergoes a gradual and complete SCO transition with $T_{1/2}$ = 218 K. No hysteresis loop was observed in **2**.

For compound **3** having a *fac*-[Fe(2-pic)$_3$]$^{2+}$ metal center, its SCO property is significantly different from that of **1** and **2**. Below 300 K, the Fe^{II} centers are in the LS state with a $\chi_M T$ value close to zero (0.02 cm^3 mol^{-1} K). Above 300 K, the $\chi_M T$ value increases gradually to 1.56 cm^3 mol^{-1} K at 342 K, then abruptly to 2.79 cm^3 mol^{-1} K at 346 K, and then increases more gradually again to a final value of 3.76 cm^3 mol^{-1} K at 400 K. This curve indicates an SCO transition with $T_{1/2}\uparrow$ = 343 K. The subsequent cooling mode provides evidence for a 10 K hysteresis loop with $T_{1/2}\downarrow$ = 333 K (Figure 5c). The effect of

DOI: 10.1021/acs.inorgchem.5b00870
Inorg. Chem. XXXX, XXX, XXX−XXX

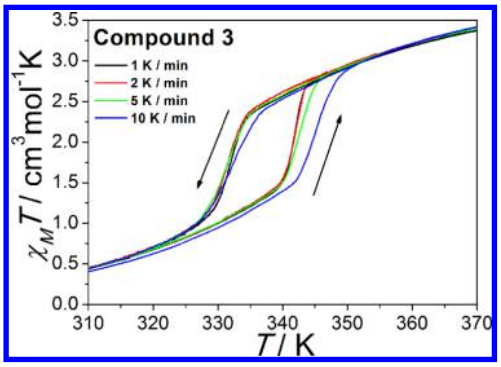

Figure 6. Temperature-dependent $\chi_M T$ plots for compound **3** recorded in the sweep mode at different temperature sweep rates (1, 2, 5, and 10 K min^{-1}). The arrows indicate the heating or cooling mode of the measurements.

the scan rate on the hysteresis width was investigated by measuring the susceptibility data at the scan rates of 1, 2, 5, and 10 K min^{-1} in the sweep mode. As shown in Figure 6, the hysteresis width is shown to be scan-rate dependent. The width of the loop is found to be slightly narrower (10 K) under slower temperature sweep rates of 1, 2, and 5 K min^{-1} compared with that (13 K) measured at 10 K min^{-1}. Anyway, the loop does not close even at the slowest temperature scan rate, indicating that it is genuine for compound **3**.

Differential Scanning Calorimetry Measurements. Furthermore, to detect the thermally induced SCO transitions in **2** and **3**, differential scanning calorimetry (DSC) measurements were performed. As for **1**, its SCO transition temperature is lower than the low-temperature limit of our DSC instrument. As shown in Figure 7, upon heating/cooling at 10 K min^{-1}, heat anomalies of endothermic/exothermic peaks were

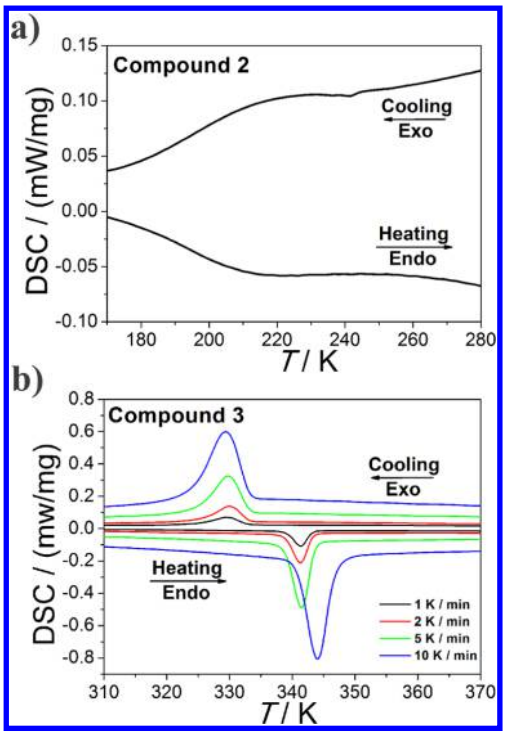

Figure 7. DSC curves of compounds **2** (a) and **3** (b) in the heating and cooling modes. The heating/cooling rate is 10 K min^{-1} for **2** and 1, 2, 5, and 10 K min^{-1} for **3**.

observed at ~216/214 and 344/330 K for **2** and **3**, respectively (broad peaks for **2** and sharp peaks for **3**). These peak temperatures agree well with the SCO transition temperatures observed in the magnetic measurements. The corresponding ΔH values were estimated to be 4.76/−3.60 and 10.19/−9.53 kJ mol^{-1} for **2** and **3**. The corresponding ΔS values were estimated to be 22.5/−16.67 and 29.64/−28.88 J K^{-1} mol^{-1} for **2** and **3**. These values are within the experimental range generally observed for the Fe^{II} SCO complexes.[3a] The observed thermal hysteresis is sweep-rate dependent for **3**; the width of the hysteresis is 14 K at 10 K min^{-1}, while narrower widths (11 K) were observed under slower temperature sweep rates of 1, 2, and 5 K min^{-1} (Figure 7b, Supporting Information, Table S8). The larger ΔH and ΔS values of compound **3** are also consistent with the fact that there is a structural phase transition of **3** accompanied by the spin state transition.

DISCUSSION

Inspired by the famous guanidinium−sulfonate inclusion compounds and our own experience on the flexible metal complex−sulfonate frameworks, we used the organosulfonates as anions and H-bond acceptors for the well-known [Fe(2-pic)$_3$]$^{2+}$ system, and three compounds were described in this work. As anticipated, all six hydrogen atoms of the three NH$_2$ groups in the [Fe(2-pic)$_3$]$^{2+}$ cation participate in the formation of extensive H bonds to the sulfonate anions. This fact justified the design principle of current work and led to the formation of the hydrogen-bonded networks.

As stated in the Introduction, the reason we are focusing on the [Fe(2-pic)$_3$]$^{2+}$ compounds is that the [Fe(2-pic)$_3$]·A$_2$·Solv materials can be regarded as prototypical examples for the study of SCO materials. In the early days of the SCO studies, investigations on these compounds revealed many important principles of the SCO properties and contributed remarkably to the development of the SCO research.[15−19] First of all, the roles of the anions and the crystallized solvents on their SCO properties were widely studied. Early in 1967, Baker et al. had discovered that different halide salts of [Fe(2-pic)$_3$]·A$_2$ (A = Cl$^-$, Br$^-$, I$^-$) exhibit different magnetic behaviors.[15] Then in the 70s and 80s, Gütlich, Strouse, Sinn, Baker et al. discovered that their SCO properties depend enormously on the crystallized solvents such as water, methanol, and ethanol.[16] Actually, more recently in 2004, Bürgi et al. also reported the engineering of the SCO properties of the [Fe(2-pic)$_3$]·Cl$_2$·Solv compounds using six different alcohol solvates.[17b] For different anions and solvents, their different size, different ability to form the hydrogen-bonded networks, and the modification of their hydrophobic part may affect their magnetic behavior. However, no obvious structure−property relationship can be made based on the reported results. Second, the [Fe(2-pic)$_3$]·A$_2$·Solv compounds have been of great value to understand the cooperative effect in the SCO compounds. The importance of the H bonds on their SCO properties was investigated through the effect of isotropic exchange in various positions of the ligand and the solvent molecules.[16e] Besides the effect of the H-bond interactions, Baker and Gütlich et al. studied in great detail the SCO properties of the solid solution [Fe$_x$Zn$_{1-x}$(2-pic)$_3$]·Cl$_2$·EtOH (x is from 0.007 to 1) using the magnetic measurements and Mössbauer spectrum.[19] Their results revealed the importance of the cooperativity in the SCO properties. Third, the [Fe(2-pic)$_3$]·A$_2$·Solv compounds contribute greatly to the understanding of the two-step SCO transitions, which is very useful for the potential application of

DOI: 10.1021/acs.inorgchem.5b00870
Inorg. Chem. XXXX, XXX, XXX−XXX

the SCO materials.[16d,17a] As a matter of fact, $[Fe(2\text{-pic})_3]\cdot Cl_2\cdot EtOH$ is the first example of the two-step transition in the Fe(II) SCO compounds.[16d] From the study of the nature of the plateau in the SCO curve of $[Fe(2\text{-pic})_3]\cdot Cl_2\cdot EtOH$, the impact of the symmetry-breaking phase transition and the order−disorder phase transition to the SCO properties was established.[17a] In addition, the structural phase transformation and its influence on the SCO properties were also studied in the $[Fe(2\text{-pic})_3]\cdot Cl_2\cdot 2\text{-PrOH}$ compound.[17c]

Interestingly, although both compounds **1** and **2** have similar *mer*-$[Fe(2\text{-pic})_3]^{2+}$ cation, their SCO properties are considerably different. While **1** has an abrupt SCO at ∼100 K, **2** has a more gradual transition with a much higher transition temperature of 218 K. Actually, the $T_{1/2}$ of **2** is the highest for all the reported $[Fe(2\text{-pic})_3]\cdot A_2\cdot Solv$ compounds of mer-configuration. For now, we cannot rationalize this difference on the transition temperatures. The methanol molecules in **1** should not be responsible for this difference, as the desolvated sample of **1** has a $T_{1/2}$ very similar to that of **1**, although the completeness of the SCO decreases to only ∼80% after desolvation. The slightly different H-bond interactions might be related to the different SCO properties. However, for the reported examples, no general trend has been formulated as yet regarding the influence of H-bonds on the SCO transition temperatures.[2c] In some compounds, it was proposed that stronger H-bonds can significantly reduce the basicity of the ligand donor group, favoring the HS states and decreasing $T_{1/2}$.[26] However, it was also suggested the H-bonds in some compounds can slightly increase the electron density on the amine/imine nitrogen of the ligand, leading to an enhanced crystal field strength and favoring the LS state.[27] As for the influence of the H-bonds on the cooperativity, it seems that H-bonds between the SCO active centers and/or the solvent molecules and/or anions should be able to efficiently transmit cooperativity and lead to more abrupt and/or hysteretic transitions. This is evidenced by many compounds where the H-bonds are responsible for the observation of wide hysteresis loops.[5] Unfortunately, there are also many reported examples with abundant H-bonds and very weak cooperativity.[28]

As for compound **3**, its SCO transition temperature is considerably higher than those of **1** and **2**. This should be mainly attributed to the different configurations of the metal centers: facial configuration for **3** and meridional configuration for **1** and **2**. For the reported examples, the facial configuration stabilized the LS state, and thus the *fac*-$[Fe(2\text{-pic})_3]\cdot Cl_2\cdot 2H_2O$ remains LS at room temperature.[16a,b] More interestingly, very wide hysteresis loop near room temperature ($T_{1/2}\downarrow$ = 204 K and $T_{1/2}\uparrow$ = 295 K) was observed in the monohydrated sample $[Fe(2\text{-pic})_3]\cdot Cl_2\cdot H_2O$, which was prepared from the partial dehydration of *fac*-$[Fe(2\text{-pic})_3]\cdot Cl_2\cdot 2H_2O$.[16a] However, detailed adiabatic heat capacity calorimetry by Sorai et al. revealed that there exist complicated phase transitions in the monohydrated sample, and the wide hysteresis loop seems to be apparent and is caused by the existence of the metastable low-spin phase.[18] Unfortunately, no direct structural information on $[Fe(2\text{-pic})_3]\cdot Cl_2\cdot H_2O$ is available, hindering the detailed study of the phase transitions. The modification of H-bond interactions might be responsible. Additionally, although it does appear unlikely, it was also proposed that the dehydration might also lead to the switching of one 2-pic ligand and convert the *fac*-$[Fe(2\text{-pic})_3]^{2+}$ cation to the *mer*-$[Fe(2\text{-pic})_3]^{2+}$ cation.[15b] In this regard, our compound **3** is the first example of the structurally characterized *fac*-$[Fe(2\text{-pic})_3]^{2+}$ motif showing SCO behavior.

Furthermore, hysteresis loop was observed, and the $T_{1/2}$ value is higher than that of the mysterious $[Fe(2\text{-pic})_3]\cdot Cl_2\cdot H_2O$. We believe that the structural phase transition, which is caused by the order−disorder transition of the OTf^- anions and the rotation of one of the OTf^- anions, should be responsible for the observation of the hysteresis loop. Experimentally, because of the higher $T_{1/2}$ values of the compounds of *fac*-configuration, it would be appealing to selectively synthesize the compounds of *fac*-$[Fe(2\text{-pic})_3]^{2+}$. However, it also seems unlikely for now. Nevertheless, compound **3** does suggest a possible manipulation of the structures of $[Fe(2\text{-pic})_3]^{2+}$ compounds using the organosulfonate anions. Because of the abundant available organosulfonate anions with different sizes, shapes, charges, and abilities to form hydrogen bonds,[10−14] we are optimistic on the synthesis of new $[Fe(2\text{-pic})_3]^{2+}$ materials. As a matter of fact, using several bisulfonates, trisulfonates, and tetrasulfonates, we have now already obtained a number of $[Fe(2\text{-pic})_3]^{2+}$ compounds with either mer- or fac- configurations or compounds of both configurations in the same structure. We noticed that the fac- compounds consistently have higher $T_{1/2}$ values. These compounds will be reported in due course.

CONCLUSIONS

In summary, we have reported here the syntheses, structures at both HS and LS states, and the magnetic properties of three $[Fe(2\text{-pic})_3]^{2+}$ compounds with different mono-organosulfonate anions. Bridged by the charge-assisted hydrogen bonds between the $[Fe(2\text{-pic})_3]^{2+}$ cation and the SO_3 group of the anions, hydrogen-bonded 3D networks or 1D columns were constructed. Although we are not sure about the causes, the $[Fe(2\text{-pic})_3]^{2+}$ cations have the mer-configurations in **1** and **2**, while it has a fac-configuration in **3**. Magnetic measurements confirmed the existence of the SCO transition for all three compounds, which is also consistent with the substantial structural modifications of the local coordination environments of the Fe^{II} centers revealed by the structural analyses at both the HS and LS states. Interestingly, compound **2** has the highest SCO transition temperature in all the compounds of *mer*-$[Fe(2\text{-pic})_3]^{2+}$ motif, and compound **3** represents the first example of the structurally characterized compound of the *fac*-$[Fe(2\text{-pic})_3]^{2+}$ motif showing SCO behavior. Depending on the different hydrogen-bond interactions, the two triflate anions in compound **3** have different order−disorder transitions, which leads to a structural phase transition and the observed thermal hysteresis in compound **3**. Although no direct connection between the geometric configuration and the specific organosulfonate anions can be established for now, the idea of the utilization of the organosulfonate to adjust the structures and SCO properties of the $[Fe(2\text{-pic})_3]\cdot A_2\cdot Solv$ compounds has been nicely demonstrated. These results shine more light on the SCO properties of the famous $[Fe(2\text{-pic})_3]\cdot A_2\cdot Solv$ compounds and open intriguing prospects for the preparation of new SCO materials. Further efforts will be aimed toward the new SCO materials with other organosulfonates of different size, charge, and functionality.

ASSOCIATED CONTENT

Supporting Information

X-ray crystallographic data in CIF format, tables for the selected bond distances, bond angles, and the details of the hydrogen bonds of compounds **1**−**3**, TGA analysis of compound **1**, PXRD and IR spectra of **1**−**3**, tables for the details of magnetic

DOI: 10.1021/acs.inorgchem.5b00870
Inorg. Chem. XXXX, XXX, XXX−XXX

measurements and DSC measurements. The Supporting Information is available free of charge on the ACS Publications website at DOI: 10.1021/acs.inorgchem.5b00870. CCDC 1057731 (**1**_90 K), 1057732 (**1**_120 K), 1057733 (**2**_120 K), 1057734 (**2**_370 K), 1057735 (**3**_120 K), 1410640 (**3**_320 K), 1410641 (**3**_360 K) and 1410642 (**3**_400 K) are the supplementary crystallographic data for this paper. They can be obtained freely from the Cambridge Crystallographic Data Center via www.ccdc.cam.ac.uk/data_request/cif.

AUTHOR INFORMATION

Corresponding Author

*E-mail: wangxy66@nju.edu.cn.

Notes

The authors declare no competing financial interest.

ACKNOWLEDGMENTS

We thank the Major State Basic Research Development Program (2013CB922102), NSFC (21101093, 21471077). This work was also supported by a Project Funded by the Priority Academic Program Development of Jiangsu Higher Education Institutions and the Fundamental Research Funds for the Central Universities (020514380006).

REFERENCES

(1) (a) Spin Crossover in Transition Metal Compounds I, II, and III. In *Topics in Current Chemistry;* Gütlich, P.; Goodwin, H. A., Eds.; Spring-Verlag: Berlin, Germany, 2004; Vols. *233*−*235*. (b) *Spin Crossover Materials: Properties and Applications;* Halcrow, M. A., Ed.; John Wiley & Sons Ltd.: New York, 2013.

(2) (a) Gütlich, P.; Hauser, A.; Spiering, H. *Angew. Chem., Int. Ed. Engl.* **1994**, *33*, 2024−2054. (b) Muñoz, M. C.; Real, J. A. *Coord. Chem. Rev.* **2011**, *255*, 2068−2093. (c) Halcrow, M. A. *Chem. Soc. Rev.* **2011**, *40*, 4119−4142. (d) Bousseksou, A.; Molnár, G.; Salmon, L.; Nicolazzi, W. *Chem. Soc. Rev.* **2011**, *40*, 3313−3335. (e) Murray, K. S.; Oshio, H.; Real, J. A. Eds. Special Issue on Spin-Crossover Complexes, *Eur. J. Inorg. Chem.* **2013**, *5*−*6*, 574−1067.10.1002/ejic.201300062 (f) Gütlich, P.; Gaspar, A. B.; Garcia, Y. *Beilstein J. Org. Chem.* **2013**, *9*, 342−391.

(3) (a) Kahn, O.; Martinez, C. J. *Science* **1998**, *279*, 44−48. (b) Liu, T.; Zheng, H.; Kang, S.; Shiota, Y.; Hayami, S.; Mito, M.; Sato, O.; Yoshizawa, K.; Kanegawa, S.; Duan, C. *Nat. Commun.* **2013**, *4*, 2826. (c) Matsumoto, T.; Newton, G. N.; Shiga, T.; Hayami, S.; Matsui, Y.; Okamoto, H.; Kumai, R.; Murakami, Y.; Oshio, H. *Nat. Commun.* **2014**, *5*, 3865. (d) Phan, H.; Benjamin, S. M.; Steven, E.; Brooks, J. S.; Shatruk, M. *Angew. Chem., Int. Ed.* **2015**, *54*, 823−827. (e) Wang, C.-F.; Li, R.-F.; Chen, X.-Y.; Wei, R.-J.; Zheng, L.-S.; Tao, J. *Angew. Chem., Int. Ed.* **2015**, *54*, 1574−1577.

(4) (a) Setifi, F.; Milin, E.; Charles, C.; Thetiot, F.; Triki, S.; Gomez-Garcia, C. J. *Inorg. Chem.* **2014**, *53*, 97−104. (b) Agusti, G.; Gaspar, A. B.; Munoz, M. C.; Real, J. A. *Inorg. Chem.* **2007**, *46*, 9646−9654. (c) Kosaka, W.; Nomura, K.; Hashimoto, K.; Ohkoshi, S. *J. Am. Chem. Soc.* **2005**, *127*, 8590−8591. (d) Arai, M.; Kosaka, W.; Matsuda, T.; Ohkoshi, S. *Angew. Chem., Int. Ed.* **2008**, *47*, 6885−6887.

(5) (a) Weber, B.; Bauer, W.; Obel, J. *Angew. Chem., Int. Ed.* **2008**, *47*, 10098−10101. (b) Weber, B.; Bauer, W.; Pfaffeneder, T.; Dirtu, M. M.; Naik, A. D.; Rotaru, A.; Garcia, Y. *Eur. J. Inorg. Chem.* **2011**, *2011*, 3193−3206. (c) Lochenie, C.; Bauer, W.; Railliet, A. P.; Schlamp, S.; Garcia, Y.; Weber, B. *Inorg. Chem.* **2014**, *53*, 11563−11572. (d) Guionneau, P.; Marchivie, M.; Bravic, G.; Létard, J. F.; Chasseau, D. *Top. Curr. Chem.* **2004**, *234*, 97−128.

(6) Ni, Z.-P.; Shores, M. P. *Inorg. Chem.* **2010**, *49*, 10727−10735.

(7) (a) Kröber, J.; Codjovi, E.; Kahn, O.; Grolière, F.; Jay, C. *J. Am. Chem. Soc.* **1993**, *115*, 9810−9811. (b) Roubeau, O. *Chem. - Eur. J.* **2012**, *18*, 15230−15244.

(8) (a) Vreugdenhil, W.; Van Diemen, J. H.; De Graaff, R. A. G.; Haasnoot, J. G.; Reedijk, J.; Van Der Kraan, A. M.; Kahn, O.; Zarembowitch, J. *Polyhedron* **1990**, *9*, 2971−2979. (b) Neville, S. M.; Halder, G. J.; Chapman, K. W.; Duriska, M. B.; Southon, P. D.; Cashion, J. D.; Létard, J. F.; Moubaraki, B.; Murray, K. S.; Kepert, C. J. *J. Am. Chem. Soc.* **2008**, *130*, 2869−2876. (c) Li, J.-Y.; Chen, Y.-C.; Zhang, Z.-M.; Liu, W.; Ni, Z.-P.; Tong, M.-L. *Chem. - Eur. J.* **2015**, *21*, 1645−1651.

(9) (a) Biradha, K.; Santra, R. *Chem. Soc. Rev.* **2013**, *42*, 950−967. (b) Nagarathinam, M.; Peedikakkal, A. M. P.; Vittal, J. J. *Chem. Commun.* **2008**, 5277−5288. (c) MacGillivray, L. R.; Papaefstathiou, G. S.; Friščić, T.; Hamilton, T. D.; Bučar, D.-K.; Chu, Q.; Varshney, D. B.; Georgiev, I. G. *Acc. Chem. Res.* **2008**, *41*, 280−291. (d) Desiraju, G. R. *Acc. Chem. Res.* **1996**, *29*, 441−449. (d) Shimizu, L. S.; Salpage, S. R.; Korous, A. A. *Acc. Chem. Res.* **2014**, *47*, 2116−2127.

(10) (a) Beatty, A. M. *Coord. Chem. Rev.* **2003**, *246*, 131−143. (b) Russell, V. A.; Evans, C. C.; Li, W.; Ward, M. D. *Science* **1997**, *276*, 575−579. (c) Holman, K. T.; Pivovar, A. M.; Ward, M. D. *Science* **2001**, *294*, 1907−1911. (d) Liu, Y.; Xiao, W.; Yi, J. J.; Hu, C.; Park, S.-J.; Ward, M. D. *J. Am. Chem. Soc.* **2015**, *137*, 3386−3392. (e) Liu, Y.; Hu, C.; Comotti, A.; Ward, M. D. *Science* **2011**, *333*, 436−440. (f) Dalrymple, S. A.; Shimizu, G. K. H. *Supramol. Chem.* **2003**, *15*, 591−606.

(11) (a) Soegiarto, A. C.; Comotti, A.; Ward, M. D. *J. Am. Chem. Soc.* **2010**, *132*, 14603−14616. (b) Evans, C. C.; Sukarto, L.; Ward, M. D. *J. Am. Chem. Soc.* **1999**, *121*, 320−325. (c) Horner, M. J.; Holman, K. T.; Ward, M. D. *Angew. Chem., Int. Ed.* **2001**, *40*, 4045−4048. (d) Horner, M. J.; Holman, K. T.; Ward, M. D. *J. Am. Chem. Soc.* **2007**, *129*, 14640−14660. (e) Holman, K. T.; Pivovar, A. M.; Swift, J. A.; Ward, M. D. *Acc. Chem. Res.* **2001**, *34*, 107−118.

(12) Xiao, W.; Hu, C.; Ward, M. D. *J. Am. Chem. Soc.* **2014**, *136*, 14200−14206.

(13) (a) Reddy, D. S.; Duncan, S.; Shimizu, G. K. H. *Angew. Chem., Int. Ed.* **2003**, *42*, 1360−1364. (b) Dalrymple, S. A.; Shimizu, G. K. H. *J. Am. Chem. Soc.* **2007**, *129*, 12114−12116. (c) Cŏté, A. P.; Shimizu, G. K. H. *Chem. Commun.* **2001**, 251−252. (d) Dalrymple, S. A.; Shimizu, G. K. H. *Chem. Commun.* **2006**, 956−958. (e) Bala, R.; Sharma, R. P.; Bond, A. D. *J. Mol. Struct.* **2007**, *830*, 198−203. (f) Dalrymple, S. A.; Shimizu, G. K. H. *J. Mol. Struct.* **2006**, *796*, 95−106. (g) Sharma, R. P.; Saini, A.; Singh, S.; Singh, A.; Venugoplalan, P.; Ferretti, V. *J. Mol. Struct.* **2010**, *969*, 155−162.

(14) (a) Wang, X.-Y.; Justice, R.; Sevov, S. C. *Inorg. Chem.* **2007**, *46*, 4626−4631. (b) Wang, X.-Y.; Sevov, S. C. *Chem. Mater.* **2007**, *19*, 4906−4912. (c) Wang, X.-Y.; Sevov, S. C. *Cryst. Growth Des.* **2008**, *8*, 1265−1270.

(15) (a) Renovitch, G. A.; Baker, W. A., Jr. *J. Am. Chem. Soc.* **1967**, *89*, 6377−6378. (b) Greenaway, A. M.; O'Connor, C. J.; Schrock, A.; Sinn, E. *Inorg. Chem.* **1979**, *18*, 2692−2695. (c) Katz, B. A.; Strouse, C. E. *Inorg. Chem.* **1980**, *19*, 658−665.

(16) (a) Sorai, M.; Ensling, J.; Hasselbach, K. M.; Gütlich, P. *Chem. Phys.* **1977**, *20*, 197−208. (b) Greenaway, A. M.; Sinn, E. *J. Am. Chem. Soc.* **1978**, *100*, 8080−8084. (c) Katz, B. A.; Strouse, C. E. *J. Am. Chem. Soc.* **1979**, *101*, 6214−6221. (d) Köppen, H.; Müller, E. W.; Köhler, C. P.; Spiering, H.; Meissner, S. E.; Gütlich, P. *Chem. Phys. Lett.* **1982**, *91*, 348−352. (e) Gütlich, P.; Köppen, H.; Steinhäuser, H. G. *Chem. Phys. Lett.* **1980**, *74*, 475−480.

(17) (a) Chernyshov, D.; Hostettler, M.; Törnroos, K. W.; Bürgi, H.-B. *Angew. Chem., Int. Ed.* **2003**, *42*, 3825−3830. (b) Hostettler, M.; Törnroos, K. W.; Chernyshov, D.; Vangdal, B.; Bürgi, H.-B. *Angew. Chem., Int. Ed.* **2004**, *43*, 4589−4594. (c) Törnroos, K. W.; Hostettler, M.; Chernyshov, D.; Vangdal, B.; Bürgi, H.-B. *Chem. - Eur. J.* **2006**, *12*, 6207−6215. (d) Chernyshov, D.; Vangdal, B.; Törnroos, K. W.; Bürgi, H.-B. *New J. Chem.* **2009**, *33*, 1277−1282.

(18) Nakamoto, T.; Bhattacharjee, A.; Sorai, M. *Bull. Chem. Soc. Jpn.* **2004**, *77*, 921−932.

(19) (a) Sorai, M.; Ensling, J.; Gütlich, P. *Chem. Phys.* **1976**, *18*, 199−209. (b) Gütlich, P.; Link, R.; Steinhäuser, H. G. *Inorg. Chem.* **1978**, *17*, 2509−2514.

(20) Hagen, K. S. *Inorg. Chem.* **2000**, *39*, 5867−5869.

DOI: 10.1021/acs.inorgchem.5b00870
Inorg. Chem. XXXX, XXX, XXX−XXX

(21) Sheldrick, G. M. *CELL_NOW;* University of Göttingen: Germany, 2006.
(22) (a) *SAINT,* Version 7.68A; Bruker AXS, Inc: Madison, WI, 2009. (b) Sheldrick, G. M. *SADABS,* Version 2008/1; Bruker AXS, Inc: Madison, WI, 2008.
(23) Sheldrick, G. M. *SHELXTL,* Version 6.14; Bruker AXS, Inc; Madison, WI, 2000−2003.
(24) (a) Guionneau, P.; Marchivie, M.; Bravic, G.; Létard, J.-F.; Chasseau, D. *Top. Curr. Chem.* **2004**, *234*, 97−128. (b) Marchivie, M.; Guionneau, P.; Létard, J.-F.; Chasseau, D. *Acta Crystallogr., Sect. B: Struct. Sci.* **2005**, *61*, 25−28.
(25) Casanova, D.; Alemany, P.; Bofill, J. M.; Alvarez, S. *Chem. - Eur. J.* **2003**, *9*, 1281−1295.
(26) Lemercier, G.; Bréfuel, N.; Shova, S.; Wolny, J. A.; Dahan, F.; Verelst, M.; Paulsen, H.; Trautwein, A. X.; Tuchagues, J.-P. *Chem. - Eur. J.* **2006**, *12*, 7421−7432.
(27) (a) Summerton, A. P.; Diamantis, A. A.; Snow, M. R. *Inorg. Chim. Acta* **1978**, *27*, 123−128. (b) Buchen, T.; Gütlich, P.; Goodwin, H. A. *Inorg. Chem.* **1994**, *33*, 4573−4576. (c) Sugiyarto, K. H.; Craig, D. C.; Rae, A. D.; Goodwin, H. A. *Aust. J. Chem.* **1994**, *47*, 869−890.
(28) (a) Kennedy, B. J.; McGrath, A. C.; Murray, K. S.; Skelton, B. W.; White, A. H. *Inorg. Chem.* **1987**, *26*, 483−495. (b) Yamada, M.; Ooidemizu, M.; Ikuta, Y.; Osa, S.; Matsumoto, N.; Iijima, S.; Kojima, M.; Dahan, F.; Tuchagues, J.-P. *Inorg. Chem.* **2003**, *42*, 8406−8416. (c) Sunatsuki, Y.; Ikuta, Y.; Matsumoto, N.; Ohta, H.; Kojima, M.; Iijima, S.; Hayami, S.; Maeda, Y.; Kaizaki, S.; Dahan, F.; Tuchagues, J.-P. *Angew. Chem., Int. Ed.* **2003**, *42*, 1614−1618. (d) Zhang, L.; Xu, G.-C.; Xu, H.-B.; Mereacre, V.; Wang, Z.-M.; Powell, A. K.; Gao, S. *Dalton Trans.* **2010**, *39*, 4856−4868.

DOI: 10.1021/acs.inorgchem.5b00870
Inorg. Chem. XXXX, XXX, XXX−XXX